RAPID COMMUNICATIONS

PHYSICAL REVIEW B VOLUME 42, NUMBER 14 15 NOVEMBER 1990-I

Scanned-angle x-ray photoemission holography with atomic resolution

G. R. Harp, D. K. Saldin, and B. P. Tonner
Department of Physics, University of Wisconsin–Milwaukee, 1900 East Kenwood Boulevard, Milwaukee, Wisconsin 53211
(Received 14 August 1990)

Two-dimensional photoemission Auger-electron diffraction patterns are shown to contain an interference pattern, which can be interpreted as a hologram to determine the three-dimensional atomic structure surrounding an atom of a particular chemical species. We demonstrate this principle by holographic reconstructions of the near-neighbor atomic structure of Cu(111) and Cu(100) surfaces from their respective diffraction patterns.

We report here the first experimental reconstructions of the local crystallographic structure surrounding a photoemitting atom using scanned-angle photoelectron holography. We find that the photoemission angular diffraction patterns from single-crystal surfaces contain interference fringes which can be used to produce an image of the near-neighbor atoms of the photoemitter by an application of a phased two-dimensional Fourier transform. These experiments show that even in the case of substrate emission, for which multiple-scattering effects may not be neglected, it is possible to directly image the local environment of a specific photoemissive chemical species with atomic resolution.

X-ray photoemission spectroscopy (XPS) is a leading tool for determining the chemical composition and the electronic properties of surfaces and interfaces. In addition to the chemical-state information found in the XPS electron energy distribution, structural information about a solid surface can be determined from a measurement of the diffraction intensity of a particular photoemission spectral feature as a function of emission direction (or equivalently, momentum).[1] The structural information of scanned-angle x-ray photoelectron diffraction (XPD) is contained in the angular anisotropy $\chi(\hat{\mathbf{k}})$ of the photoemission intensity from a specific chemical state at a fixed kinetic energy.[2]

For kinetic energies above a few-hundred electron volts, the structure of the photoemission anisotropy $[\chi(\hat{\mathbf{k}})]$ is dominated by final-state diffraction. Initial-state effects are of less importance at high kinetic energy, so that valence electrons, core levels, and Auger electrons all show similar features in the anisotropy.[3] It is commonly observed that there are strong intensity maxima in $\chi(\hat{\mathbf{k}})$ for emission directions parallel to low-index crystallographic directions, due to forward scattering along atom chains in the sample.[1,4–6]

The forward-scattering peaks in $\chi(\hat{\mathbf{k}})$ have been used to determine bond angles in unknown structures in a qualitative way.[7] While quite useful in determining the general characteristics of a structure, this approach is limited in accuracy and does not provide information about bond distances. An obstacle to the widespread application of XPD for structure determination in the past has been that a quantitative interpretation of $\chi(\hat{\mathbf{k}})$ required a comparison of experimental measurements to a computer simulation of the scattering from various model structures.[1,6] In this work we demonstrate a direct method of transforming measured diffraction patterns to produce images of near-neighbor atom positions surrounding the emitter atom. Combined with the well-known chemical specificity of XPS, this method can be used to determine the local symmetry and bond distances of an atom in a selected chemical state.

This new approach to XPD rests on recognizing that $\chi(\hat{\mathbf{k}})$ can be viewed as a Fraunhoffer hologram.[8] The incident x ray creates an outgoing electron wave centered on an atomic site. This direct wave from the photoemitter to the detector can be viewed as a "reference" wave. It scatters coherently from neighboring atoms, forming the "object" wave. This object wave contains the superposition of all elastic single- and multiple-scattering paths from the emitter atom to the detector. The interference between the object wave and the reference wave determines the photoemission angular anisotropy, which constitutes the hologram.

Simulations of the photoelectron diffraction from an adsorbate atom by Barton[9] showed that backscattered electron-diffraction patterns could be treated as holograms to numerically reconstruct the positions of near-neighbor substrate atoms below the adsorption site. However, the low electron kinetic energies necessary for strong backscattering are incompatible with high spatial resolution in a holographic transform. In a previous publication, we reported[10] that this limitation could be overcome by utilizing higher electron kinetic energies, combined with sample geometries that enhance forward scattering. These conditions are particularly favorable for imaging the sites of atoms below the outermost surface layer. We demonstrated the three-dimensional reconstruction of near-surface atom positions using Kikuchi-scattering diffraction patterns[10] from Cu(100).

In order to perform a holographic reconstruction from photoemission data, it is necessary to accumulate the anisotropy function $\chi(\hat{\mathbf{k}})$ over a substantial region of the 2π steradian solid angle of emission. For this purpose, we have measured the two-dimensional $3p$ photoelectron and L_3VV Auger-electron anisotropy from single-crystal surfaces of Cu(001), Cu(110), and Cu(111), as well as the $4f$ photoemission anisotropy for Ir(111). Each of these diffraction patterns has been analyzed as a hologram and

compared to the known crystal structure. We report here the results from the Cu(001) and Cu(111) Auger emission experiments. The successful reconstruction of crystal structure for different materials and surface orientations shows the generality of the method. In the case of Cu(001) Auger holography, the reconstructed images are remarkably similar to the reconstructions reported earlier using reflection Kikuchi electrons.[10] This result can be taken as further confirmation that Auger-electron and Kikuchi-electron angular distributions are primarily determined by final-state diffraction at these kinetic energies. The reconstruction of primary photoelectron holograms is more complex, due to the influence of photon polarization matrix-element effects; this topic will be treated in a subsequent publication.

Figure 1 shows the *LVV* Auger-electron diffraction pattern from Cu(001), excited by Mg $K\alpha$ x-rays and measured at a kinetic energy of 914 eV.[4] The angle between the incident x-ray beam and the detected electron is constant ($\sim 70°$), and the sample is rotated so as to vary the electron polar angle with respect to the sample normal. The complete angular diffraction pattern is assembled from individual polar-angle scans for different crystal azimuths. Since the measured angular distributions span the range of angles between two mirror planes of the crystal, it was possible to construct the angular intensity distribution over the entire azimuthal range by successive mirror operations.[11]

The bright spots and channels that are visible to the eye in the Auger diffraction pattern (Fig. 1) are primarily due to the forward scattering of electrons along atom chains in the crystal. These features are useful in themselves, and can be used as a fingerprint of different crystal structures.[7] However, the location of these high-intensity features depends only on bond angles in the crystal, so that no information about bond lengths can be inferred. As we demonstrate here, this missing information is provided by a holographic interpretation of the electron angular distribution, which results in a three-dimensional reconstruction of atomic scatterers near the emitting atom.

To prove that measured photoemission angular distributions are holograms, we have performed reconstructions using computer techniques previously described.[10,12] To transform the photoemission anisotropy we use the Helmholtz-Kirchhoff integral:[13]

$$A(\mathbf{r}) = \int \chi(\hat{\mathbf{k}}) e^{-ik\hat{\mathbf{k}}\cdot\mathbf{r}} d\hat{\mathbf{k}} . \tag{1}$$

This is a two-dimensional integral over the photoemission angular-distribution "surface," with the anisotropy normalized so that $\int \chi(\hat{\mathbf{k}}) dk_x\, dk_y = 0$. This straightforward Fourier integral results in a three-dimensional intensity distribution in real-space coordinates, $|A(\mathbf{r})|^2$, which is the reconstructed image. For $kr \gg 1$, the reconstruction amplitude $A(\mathbf{r})$ is large only for $\mathbf{r} = \pm \mathbf{r}_j$, where $\mathbf{r}_j$ are the atomic positions.[9]

In order to display the information in the reconstructed image, we plot two-dimensional sections of $|A(\mathbf{r})|^2$, which correspond to the expected positions of the atomic planes. Figure 2 is a section parallel to the sample surface, in a (001) plane containing the nearest-neighbor atoms lying between the photoemitter and the detector. The black crosses mark the locations of the atoms in an ideal single crystal of Cu(001). The agreement between the intensity maxima of the holographic reconstruction and the expected atomic positions is very good.

An illustration of the three-dimensional character of the holographic reconstruction is shown in Fig. 3. Here, we plot a section of the reconstruction perpendicular to the surface of the crystal, in a (110) plane containing the nearest-neighbor atoms. The black crosses mark the loca-

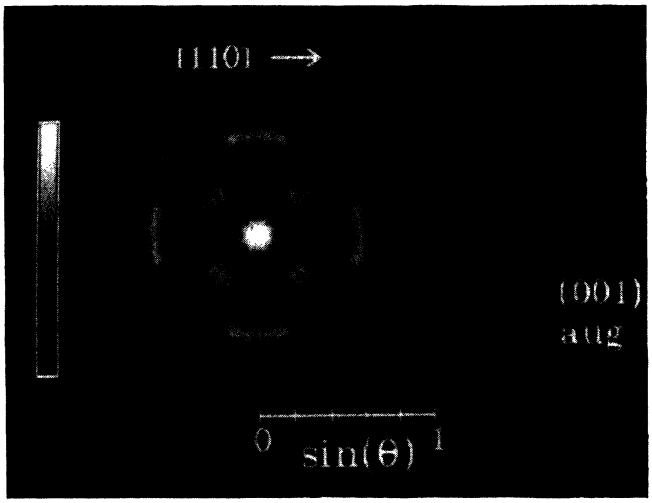

FIG. 1. Measured photoemission Auger-electron angular anisotropy at 914 eV from Cu(001). The electron interference pattern is displayed in stereographic projection as a function of parallel momentum, with zero momentum (normal emission) at the center. The arrow shows the orientation of the crystallographic axis, and the scale gives the sine of the polar angle.

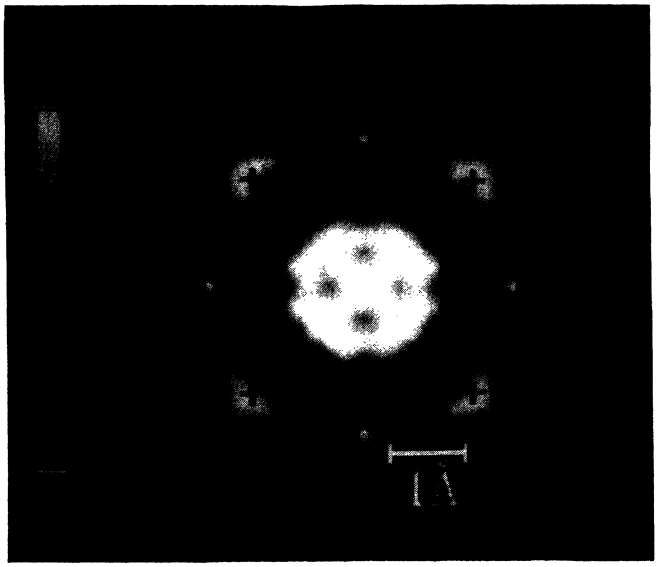

FIG. 2. Holographic reconstruction of the atom positions from the angular distribution of Fig. 1, corresponding to a plane of atoms between the emitter atom and the detector. The crosses mark the locations of atoms in the ideal crystal.

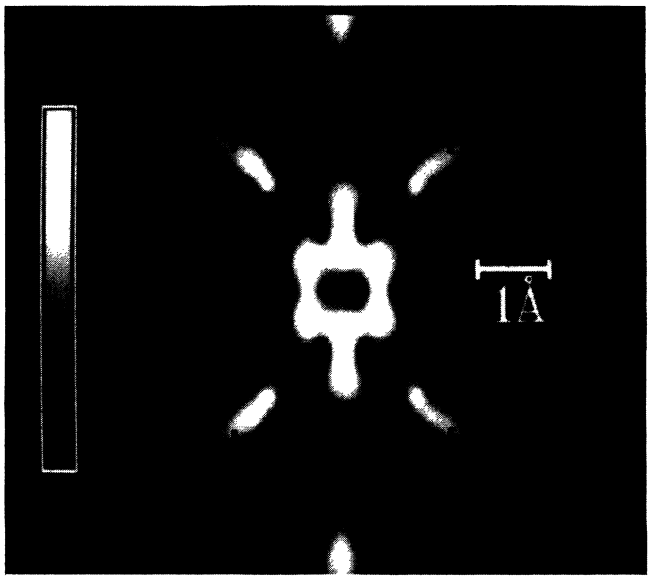

FIG. 3. A view in a plane perpendicular to the crystal surface from the holographic reconstruction of the data of Fig. 1. The crosses mark the locations of atoms in the ideal lattice. The elongated shape of the atom image is due to a reduction in resolution parallel to the electron emission direction.

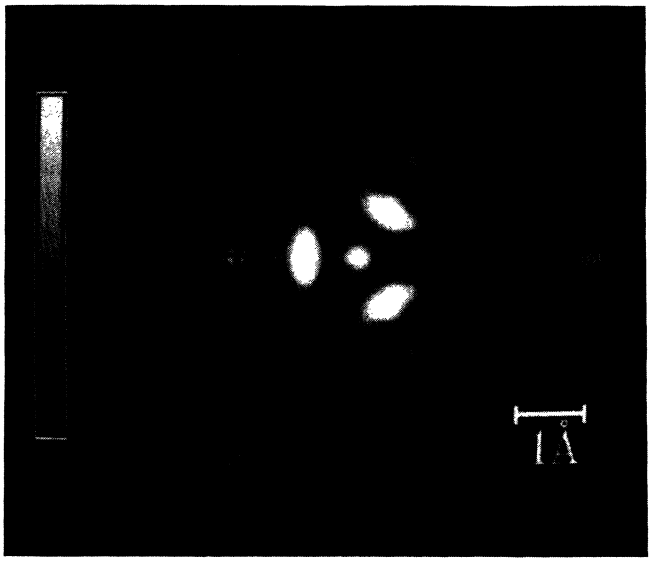

FIG. 4. Holographic reconstruction of the atom positions from the angular distribution of L_3VV Auger electrons from a Cu(111) surface. Shown here is the plane, lying between the emitting atom and the detector, that contains the three nearest-neighbor atoms. The crosses mark the locations of atoms in the ideal lattice.

tion of atoms in the ideal crystal. While the resolution of the hologram is not as high in the perpendicular direction, the intensity maxima are still in good agreement with the expected atomic positions.

Some general factors affecting the quality of photoemission holographic images can be assessed from our experience with these single-crystal test cases. Since the forward-scattering features of the photoemission diffraction pattern are correlated with specific real-space *directions,* the location of these features in angle space does not change with electron energy. The interference fringes that constitute the photoemission hologram, however, *must* change their angular position as the electron kinetic energy varies. For example, the angular half-width of the first fringe maximum is of order $\Delta\theta_{1/2}\sim 25°$ for a two-atom chain at a kinetic energy near 1000 eV.[1,14] At lower energies, the fringe spacing increases, and the fringe visibility decreases, due to a reduction in the magnitude of the enhancement factor $\chi(\hat{\mathbf{k}})$.

The diffraction-limited resolution of the image of an atom depends on the range of momentum $\Delta\mathbf{k}$ for which strong fringes contribute to the reconstruction of that atom. Under conditions of strong forward scattering, the holographic image of an atom at $\mathbf{r}_j$ results primarily from interference fringes confined to a conical region of the diffraction hemisphere centered on the internuclear direction $\hat{\mathbf{r}}_j$. If the half angle of this cone is $\Delta\theta_{1/2}=25°$, then the image resolution can be estimated from the uncertainty principle to be of order $\Delta r_\perp = 1/2k\sin(\Delta\theta_{1/2})\sim 0.1$ Å in the direction *perpendicular* to $\mathbf{r}_j$, and $\Delta r_\parallel = 1/k[1-\cos(\Delta\theta_{1/2})]\sim 0.7$ Å in the direction *parallel* to the internuclear axis. These values are in good agreement with the observed resolution in Figs. 2 and 4. The resolution parallel to $\hat{\mathbf{r}}_j$ is always poorer than in the perpendicular direction, leading to the tubular shapes seen in the vertical plane reconstructions.

In contrast, the experimental angular resolution $\delta\theta$ determines how far from the emitter atom the reconstruction is reliable. That is, $r_{\max}\sim\pi/|\mathbf{k}|\delta\theta$. To successfully image the nearest-neighbor atoms, the experimental angular resolution need only be small compared to the angular half-width of the interference fringe spacing.

We have applied the method of holographic reconstruction to photoelectron and Auger-electron emission from a number of single-crystal surfaces. The results from

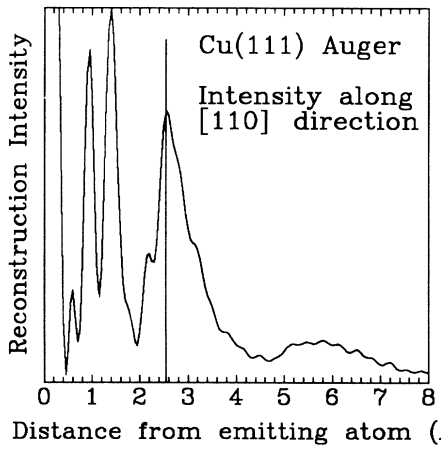

FIG. 5. Intensity of the reconstruction from the Cu(111) Auger diffraction pattern, along a line in the [110] direction of the crystal, starting at the location of the emitting atom. The expected position of a nearest-neighbor atom is marked by the vertical line.

Cu(111) are included here to demonstrate the generality of the approach. The photoemission Auger-electron angular distribution can be found in Ref. 6. The reconstruction image in a plane parallel to the surface, containing the nearest-neighbor atoms above the emitter, is shown in Fig. 4. In this case, there also appears to be a local intensity maximum at the correct location of the next-nearest-neighbor atoms in the plane (these are not marked in the figure).

The accuracy of the holographic technique can be demonstrated in the following way. The reconstruction algorithm produces a three-dimensional intensity distribution. We can plot this intensity along an arbitrary vector in space. In Fig. 5, for example, we plot the intensity from the reconstruction of Cu(111) data, along a line corresponding to the [110] direction of the crystal. This direction is the nearest-neighbor direction of the fcc lattice. The vertical line in Fig. 5 is placed at the ideal atom bond distance of 2.55 Å. The holographic intensity has a local maximum at this distance. The feature near 1.8 Å can easily be excluded on physical grounds.

A photoemission hologram averages over all emitting atoms that produce electrons of the same kinetic energy. As such, the hologram is an atomic-resolution image of the average structure of chemically equivalent emitters in the domain illuminated by the x-ray beam. This domain size can be made smaller than one micrometer in diameter, using x-ray optics and synchrotron radiation.[15] In addition, the tunability of synchrotron radiation will enable holograms to be taken at several energies. Averaging reconstructions of holograms taken at different energies may improve the resolution of the reconstruction and help identify and eliminate artifacts. Auger-electron holography can also be accomplished with a high-energy electron beam as the excitation source, so that the emitting domain size can be made comparable to the size of the incident focused electron beam.

This work was supported in part by the National Science Foundation, Grant No. DMR-88-05171.

[1]For a review of angle-resolved photoelectron diffraction, see C. S. Fadley, in *Synchrotron Radiation Research: Advances in Surface Science,* edited by R. Z. Bachrach (Plenum, New York, 1990).

[2]An alternative form of photoelectron diffraction measures the *energy* dependence of emission intensity at fixed angle (see Ref. 1). This form of XPD is analogous to extended x-ray-absorption fine structure, and cannot be used to produce a three-dimensional real-space image.

[3]J. Osterwalder, T. Greber, S. Hufner, and L. Schlapbach, Phys. Rev. B **41**, 12495 (1990).

[4]H. Li and B. P. Tonner, Phys. Rev. B **37**, 3959 (1988).

[5]Few full-symmetry photoemission isointensity contour plots have been published. Two examples are found in R. J. Baird, C. S. Fadley, and L. F. Wagner, Phys. Rev. B **15**, 666 (1977); and M. Owari, M. Kudo, Y. Nihei, and H. Kamada, Jpn. J. Appl. Phys. **24**, L394 (1985).

[6]X. D. Wang, Z.-L. Han, B. P. Tonner, Y. Chen, and S. Y. Tong, Science **248**, 1131 (1990).

[7]Hong Li and B. P. Tonner, Phys. Rev. B **40**, 10241 (1989).

[8]A. Szöke, in *Short Wavelength Coherent Radiation: Generation and Applications,* edited by D. T. Attwood and J. Boker, AIP Conference Proceedings No. 147 (American Institute of Physics, New York, 1986).

[9]John J. Barton, Phys. Rev. Lett. **61**, 1356 (1988).

[10]G. R. Harp, D. K. Saldin, and B. P. Tonner, Phys. Rev. Lett. **65**, 1012 (1990).

[11]The data processing of photoemission diffraction patterns is described in Ref. 4. Note that the boundary conditions at the mirror planes are determined by measurement, and not by the data processing.

[12]D. K. Saldin and P. L. de Andres, Phys. Rev. Lett. **64**, 1270 (1990).

[13]See for example, M. Born and E. Wolf, *Principles of Optics* (Pergamon, New York, 1965), Sec. 8.3.

[14]H. C. Poon and S. Y. Tong, Phys Rev. B **30**, 6211 (1984).

[15]J. Kirz and H. Rarback, Rev. Sci. Instrum. **56**, 1 (1985).

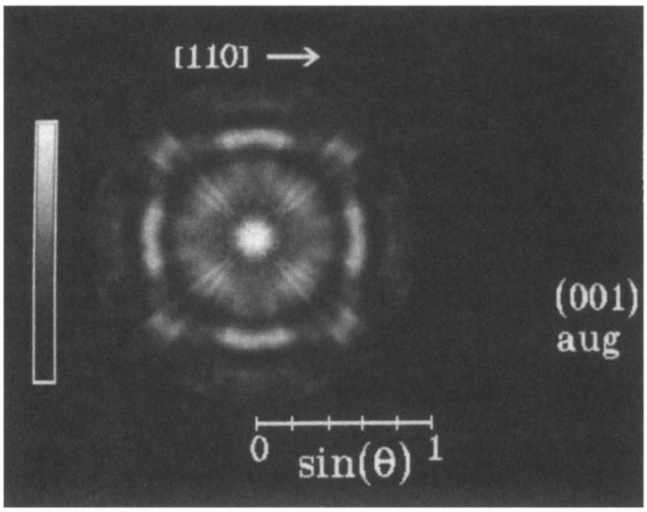

FIG. 1. Measured photoemission Auger-electron angular anisotropy at 914 eV from Cu(001). The electron interference pattern is displayed in stereographic projection as a function of parallel momentum, with zero momentum (normal emission) at the center. The arrow shows the orientation of the crystallographic axis, and the scale gives the sine of the polar angle.

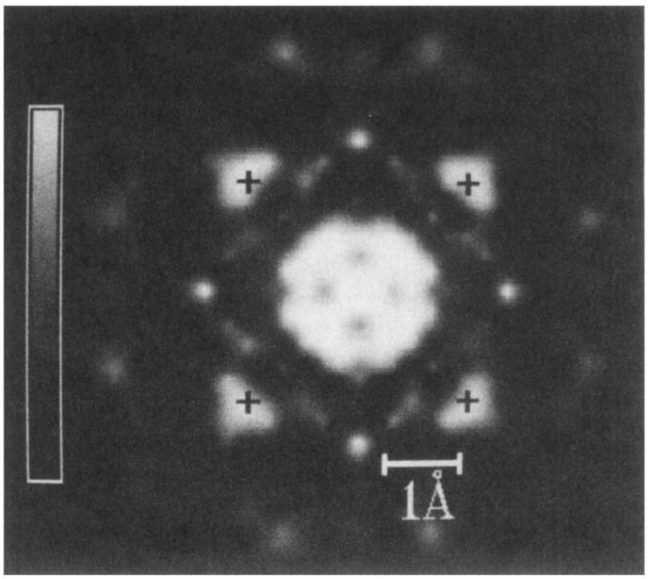

FIG. 2. Holographic reconstruction of the atom positions from the angular distribution of Fig. 1, corresponding to a plane of atoms between the emitter atom and the detector. The crosses mark the locations of atoms in the ideal crystal.

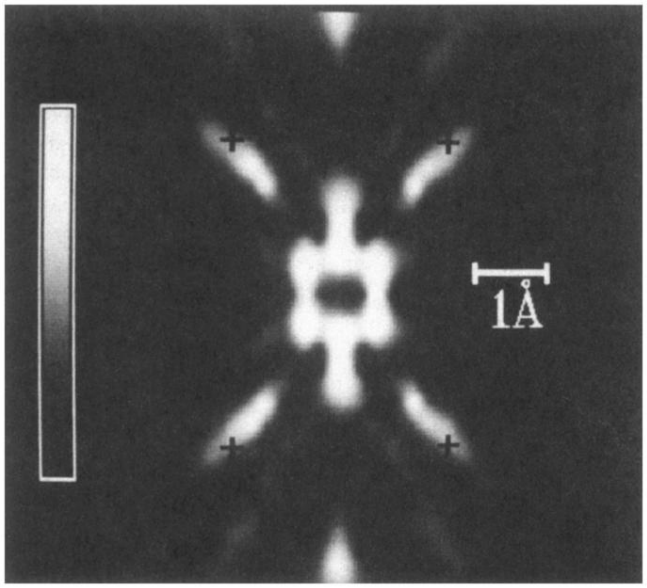

FIG. 3. A view in a plane perpendicular to the crystal surface from the holographic reconstruction of the data of Fig. 1. The crosses mark the locations of atoms in the ideal lattice. The elongated shape of the atom image is due to a reduction in resolution parallel to the electron emission direction.

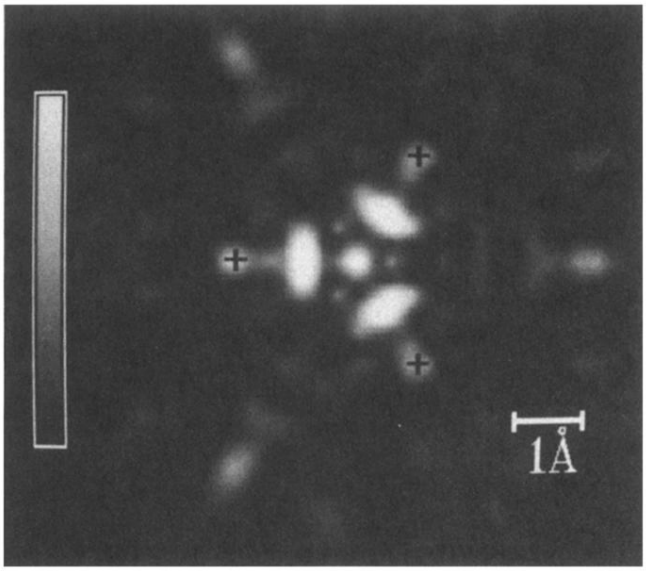

FIG. 4. Holographic reconstruction of the atom positions from the angular distribution of L_3VV Auger electrons from a Cu(111) surface. Shown here is the plane, lying between the emitting atom and the detector, that contains the three nearest-neighbor atoms. The crosses mark the locations of atoms in the ideal lattice.